Synthesis and structure of PMN–PT ceramic nanopowder free from pyrochlore phase

M. Ghasemifard, S.M. Hosseini *, Gh.H. Khorrami

Department of Physics (Materials and Electroceramics Laboratory), Ferdowsi University of Mashhad, Mashhad, Iran

Abstract

Single-phase perovskite 0.65PMN–0.35PT nanopowders were synthesized at low temperature by the auto-combustion method. PMN–PT powder with 1 mol% of excess $Pb(NO_3)_2$ was prepared from the constituent nitrates and alkoxide materials. Perovskite PMN–PT powders without any pyrochlore phase were obtained after heat treatment at 850 °C. The average particles diameter is estimated to be around 25 nm. The formation of perovskite phase and the optical constants of powders have been estimated using Fourier transform infrared (FTIR) spectroscopy.
© 2009 Elsevier Ltd and Techna Group S.r.l. All rights reserved.

Keywords: A. Sol–gel processes; C. Optical properties; D. PMN–PT

1. Introduction

The relaxor ferroelectric lead magnesium niobate $Pb(Mg_{1/3}Nb_{2/3})O_3$ (PMN) exhibits typical relaxor-type ferroelectric properties that have been intensively studied for both fundamental and practical reasons [1]. The dielectric properties of PMN can be enhanced by the addition of ferroelectric $PbTiO_3$ (PT). The solid solution of $(1 - x)$PMN–xPT (PMN–PT) forms between PMN and $PbTiO_3$, with a morphotropic phase boundary (MPB) located in the composition range $0.27 < x < 0.34$. The MPB is frontier between the rhombohedral (relaxor side) with space group $R3m$ and tetragonal (ferroelectric side) with space group $P4mm$ phases as illustrated in Fig. 1. The structure of this complex system contains two monoclinic phases with space group Cm (M_A type) and Pm (M_c type) stable in the composition range $0.27 < x < 0.30$ and $0.31 < x < 0.34$, respectively [2]. This is similar to the monoclinic phase observed in $PbZr_{1-x}Ti_xO_3$ (PZT) system in the vicinity of $x = 0.47$ [3]. Single crystal of PMN–PT with compositions near the MPB have been reported to exhibit very high piezoelectric coefficients ($d_{33} > 2500$ pC/N), extremely large piezoelectric strains (>1.7%) and very high electro-

mechanical coupling factors ($k_{33} > 92\%$). These values are significantly higher than those provided by the best lead zirconate titanate (PZT) based piezoceramics (600–700 pC/N and 0.17%) [4,5].

The PMN–PT ceramics have been widely studied in the area of electronic ceramics by many investigators. Alguerò et al. [6] have been prepared piezoelectric PMN–PT ceramics with 0.2 and 0.35PT from mechanochemically activated powders. The 0.35PT ceramics presented a first order ferroelectric–paraelectric transition at 171 °C and a complex transverse piezoelectric coefficient of $-(181.8 - i3.6)$ pC/N and d_{33} of 570 pC/N at room temperature. Kong et al. [7] have been prepared PMN–PT ceramic from nano-sized powder produced by a high-energy ball milling process.

Regarding the thin film of PMN–PT, there are many attempts to find alternatives which are less expensive for possessing of these materials. Lead–magnesium–niobate–lead–titanate thin films (PMN–PT) have been also prepared on Si and $Pt/Ti/SiO_2/$ Si substrates by MOCVD using ultrasonic nebulization [8]. Udayakumar et al. [9] have prepared the PMN–PT thin film of the morphotropic phase boundary composition through the sol–gel spin-on technique.

Synthesis the single-phase of PMN–PT powder and free from pyrochlore phase is the main task of investigators to fabricate a good device. Kwon et al. [10] have fabricated perovskite 0.65PMN–0.35PT powder at 600 °C for 1 h using

---

* Corresponding author. Tel.: +98 511 8435723; fax: +98 511 8796426.
E-mail address: sma_hosseini@yahoo.com (S.M. Hosseini).
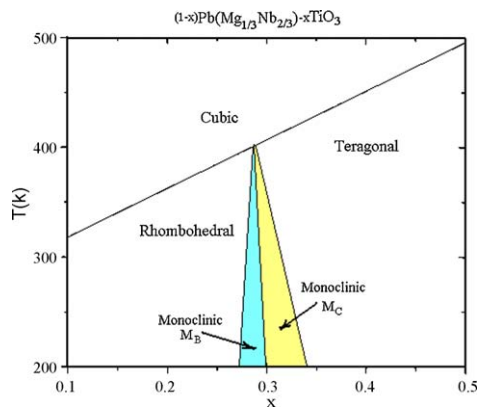
Fig. 1. Phase diagram of the PMN–PT. The diagonally shaded area represents the monoclinic (*M*) phase region [2].

Fig. 2. Flow diagram for PMN–PT powder preparation procedure.

fine starting materials, which is the lowest temperature so far have been reported. Their fine-particle characteristics resulted in rapid direct transformation via solid-state diffusion. Luo et al. [11] have reported a double precursor solution coating method to obtain the PMN–PT powder at temperature of 900 °C.

In this work, we introduce a simple way to fabricate pure perovskite 0.65PMN–0.35PT powder with inexpensive material in sub-micrometer size by auto-combustion method. The results of an X-ray diffraction study showing unambiguous evidence of a monoclinic phase, which is stable between the rhombohedral and tetragonal phases near the MPB and free from pyrochlore phase.

Despite the number of papers already published on the synthesis of PMN–PT powders but the optical properties of perovskite PMN–PT nanopowders have rarely been studied. Moreover, the optical characterization gives valuable information about the structural parameters of the powder. However, in this paper the optical properties are discussed and some optical constants of synthesized PMN–PT powders have been evaluated from Kramers–Kronig analysis using FTIR spectra data.

2. Experimental

The raw materials used in this experiment were lead(II) nitrate [$Pb(NO_3)_2$], magnesium acetate [$(CH_3COO)_2Mg \cdot 4H_2O$], niobium ammonium oxalate [[$NH_4[Nb(C_2O_4)_2(H_2O)] \cdot 4H_2O$] and titanium isopropoxide $Ti[OCH(CH_3)_2]_4$. Aqueous solutions of single cation Pb^{+2} were prepared by dissolving lead(II) nitrate in distilled water. For preparation of Ti^{+4} we dissolve titanium(IV) isopropoxide in mixture of nitric, citric acid and hydrogen peroxide. A proxo-citrate–niobium complex (NH_4)[$NbO(O_2)(C_6H_4O_7)$] was prepared from niobium ammonium oxalate, citric acid, nitric acid and ammonia. The solutions of lead, titanium, niobium and magnesium were added to the aqueous solution of citric acid under continuous stirring at 65–70 °C and maintaining the pH at 7 by the addition of ammonium hydroxide. The peroxo-citrato-nitrate sols of PMN–PT were heated at about 80 °C to evaporate all the water and to obtain the gel. PMN–PT powder was produced by
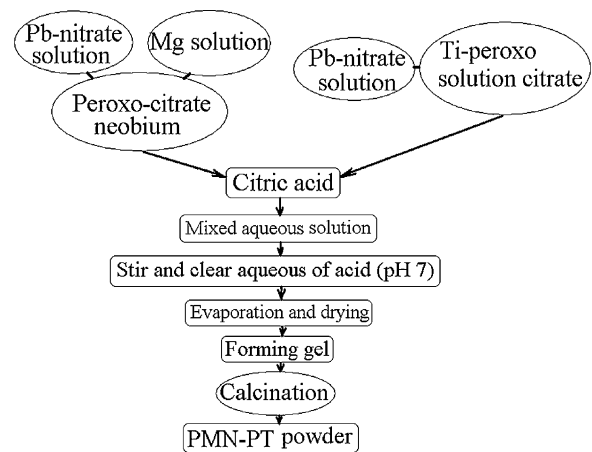
the citrate–nitrate gel auto-combustion technique. The flow diagram of the powder processing methods employed in this study is shown in Fig. 2.

After auto-combustion of the gels, the resultant powders were calcinated at different temperatures to obtain the desired Single-phase powders. The phase formation and orientation of PMN–PT powder were investigated using X-ray diffraction analysis in the range (4–60°) with CuK_α radiation. Fourier transform infrared spectroscopy (FTIR) was used to monitor the phase change of organic group in the wavenumber range 400–5000 cm^{-1}.

3. Results and discussion

3.1. Phase analysis and particles size

X-ray diffraction patterns of PMN–PT powders (heating rate: 2 °C/min from room temperature to various temperatures ranging from 700 °C to 850 °C for 2 h) are shown in Fig. 3. The presence of a monoclinic phase at temperature of 850 °C can be identified from this figure. The XRD results also reveal the existence of a perovskite-type phase for the gel-combustion
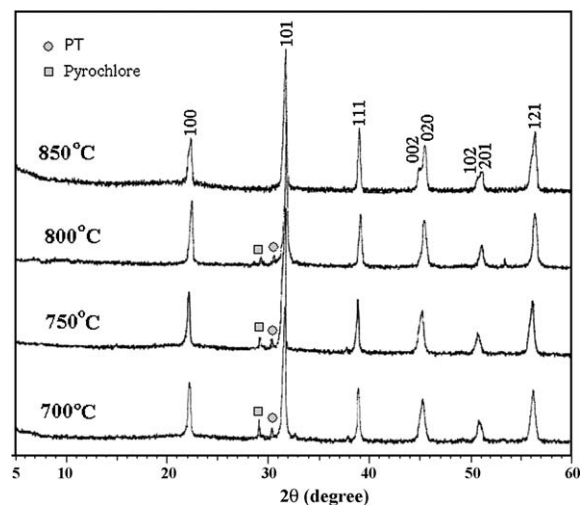
Fig. 3. XRD spectra of samples of the PMN–PT calcined at different temperatures.

Table 1
Structural result for 0.65PMN–0.35PT powders calcinated at different temperatures.

Temperature (°C)	2θ (°)	d_{hkl}	hkl	Structure	Lattice parameter (Å)
700	45.16	2.006	0 0 2	Rhombohedral	$a = 4.014$
	50.78	1.796	0 1 2		$\alpha = 90.02°$
750	45.18	2.005	0 0 2	Rhombohedral	$a = 4.010$
	50.80	1.797	0 1 2		$\alpha = 90.03°$
800	45.20	2.004	0 0 2	Rhombohedral	$a = 4.015$
	50.83	1.795	0 1 2		$\alpha = 90.02°$
850	45.43	2.022	0 0 2	Rhombohedral and monoclinic	$a = 4.014$
	45.78	1.995	0 2 0		$\alpha = 90.02°$
	50.59	1.803	1 0 2		$a = 3.99$
	51.04	1.788	2 0 1		$b = 3.98$
					$c = 4.04$
PMN–xPT for $x = 0.35$ [2]				Rhombohedral	$a = 4.023$
					$\alpha = 89.85°$
PMN–xPT for $x = 0.35$ [13]				Monoclinic	$a = 4.0344$
					$b = 3.9873$
					$c = 4.0092$
PMN–xPT for $x = 0.32$ [12]				Monoclinic	$a = 4.0183$
					$b = 4.0046$
					$c = 4.0276$

method in all temperatures. At temperatures lower than 850 °C the samples still contain some pyrochlore phase but at 850 °C completely have disappeared. The structural results for PMN–PT in this work and the values obtained by the others are summarized in Table 1. The calculated lattice parameters obtained in this work are consistent with the reported values for 0.65PMN–0.35PT bulk ceramic [2,13].

The typical TEM image of the PMN–PT powder calcinated at temperatures of 800 °C prepared by the auto-combustion method is shown in Fig. 4. From TEM analysis the primary particle size of the powders can be determined. The primary particles size of the PMN–PT powder was fount to be approximately 25 nm in diameter.

3.2. FTIR Spectrum

FTIR spectroscopy was used in order to monitor the transformation of precursor solutions during the thermal reactions leading to the perovskite oxide powders. Fig. 5 shows the FTIR spectra of the PMN–PT powders in the range of 5000–400 cm^{-1} treated at different temperature of 700 °C, 750 °C, 800 °C and 850 °C for a period of 2 h. In this frequency interval, a broad band was observed for each spectrum from 850 cm^{-1} to 590 cm^{-1} with a maximum absorbance in the vicinities of 596 cm^{-1}. This peak has been associated with the vibration of B–O (B = Mg, Nb and Ti) bonds in the systems.

Fig. 4. TEM micrograph of the prepared PMN–PT powders at 800 °C.
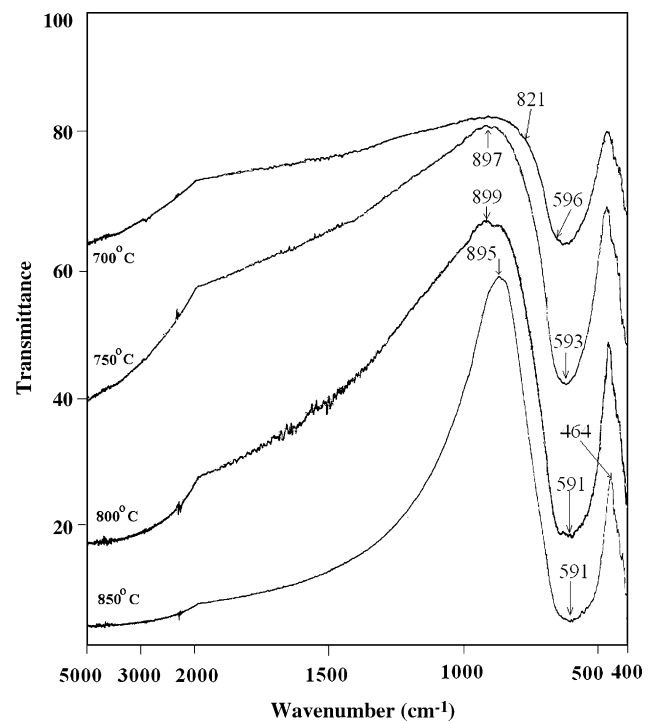
Fig. 5. FTIR spectra of PMN–PT powders treated at different temperatures of 700 °C, 750 °C, 800 °C and 850 °C.

The IR spectrum for PMN–PT is similar to the most other ABO$_3$-type perovskite compounds that present four distinct vibration modes [14,15]. In Fig. 5 two absorption bands were observed. The higher frequency asymmetric band, ν_1-streching, extends from 850 cm^{-1} to 590 cm^{-1}, with a center in the vicinities of 596 cm^{-1}. This observed infrared spectrum band is a composition of ν_1-NbO$_3$, ν_1-TiO$_3$ and ν_1-MgO$_3$ stretching normal vibration modes along the spontaneous polarization in PMN–PT structure. There is a little change in ν_1 as temperature of calcinations was increased. This band, ν_1, is associated to BO$_6$ octahedron bond and indicates the formation of a perovskite phase starts to take place for all calcinated temperatures and starts to increase in proportion as the temperature increases. Bands associated with Pb ions were not observed in the mid-infrared spectra because of their heavy masses.

The lower frequency band, ν_2-bending, extends from 400 cm^{-1} which is behind the available experimental range at 400 cm^{-1} is assigned to B–O bending normal vibration. However, the other two bands, ν_3-cation-(BO$_3$) lattice mode and ν_4-bending vibrations are below the available experimental frequency range (5000–400 cm^{-1}) used in this work [16].

3.3. Evaluation of the optical constants

We used Kramers–Kronig analysis to evaluate the optical constants of PMN–PT powders prepared by gel-combustion method using FTIR spectra data [17,18]. The IR spectra (Fig. 5) show the absorbance values are less than 67%. As a result, the absorption coefficient (α), in the strong absorption region where the envelop method [19] is not valid, should be evaluated from the optical transmittance data using Lambert's principle [20,21]

$$\alpha = -\left(\frac{1}{t}\right)\ln T \tag{1}$$

where T is the transmittance and t is the thickness of the KBr pellet prepared for IR measurements or diameter of nanoparticle. Knowing both t and T, we may calculate the absorption

coefficient from Eq. (1). The absorption coefficient as a function of photon energy can be expressed from well known relation as [22]:

$$(\alpha h \upsilon)^2 = C\left(\frac{hc}{\lambda} - E_g\right) \tag{2}$$

where C is a constant, α is the absorption coefficient, (hc/λ) is the incident photon energy and E_g is the band gap energy. By plotting $(\alpha h \upsilon)^2$ versus (hc/λ), E_g can be evaluated from the extrapolated linear portion of the plot. The complex refractive index can be calculated from the following equation [23]:

$$\tilde{n}(\omega) = n(\omega) + ik(\omega) \tag{3}$$

where n is the real and k is the imaginary part of complex refractive index. The refractive index and the extinction coefficient can be calculated from following relations:

$$n(\omega) = \frac{1 - R(\omega)}{1 + R(\omega) - 2\cos\varphi(\omega)\sqrt{R(\omega)}} \tag{4}$$

$$k(\omega) = \frac{2\sin\varphi(\omega)\sqrt{R(\omega)}}{1 + R(\omega) - 2\cos\varphi(\omega)\sqrt{R(\omega)}} \tag{5}$$

where R is the reflectance and φ is the phase change at a particular wavenumber between the incidences and the reflected signal that obtain from following equation:

$$\varphi(\omega) = -\frac{\omega}{\Pi}\int\limits_0^\infty \frac{\ln R(\omega') - \ln R(\omega)}{\omega'^2 - \omega^2}d\omega' \tag{6}$$

For calculating $\varphi(\omega)$ several extrapolation approaches have been evaluated and reported [24–26]. We have calculated $\varphi(\omega)$ by Maclaurin's method [27] from Eq. (7), this method is rather accurate, but it needs double Fourier transform and the calculation takes a relatively longer time.

$$\varphi(\omega_g) = \frac{2\omega_g}{\pi} \times 2h \times \sum_i \frac{\ln(\sqrt{R(\omega)}}{\omega_i^2 - \omega_g^2} \tag{7}$$
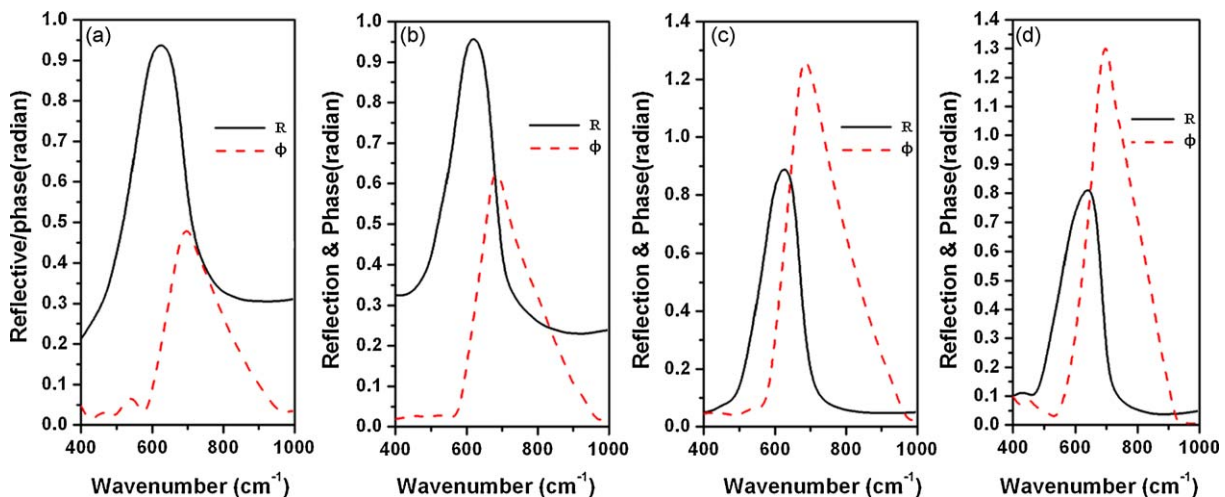
Fig. 6. Reflectance (solid line) and the phase change (dash line) spectrum PMN–PT powder calcinated at different temperatures: (a) 700 °C, (b) 750 °C, (c) 800 °C and (d) 850 °C.
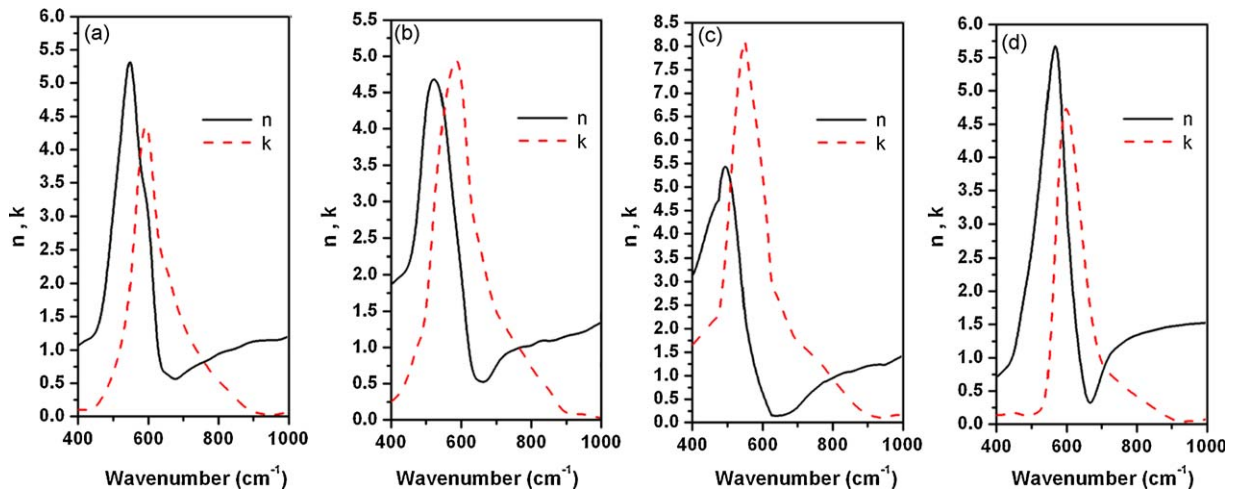
Fig. 7. The refractive index (solid line) and extinction coefficient (dash line) for PMN–PT powder calcinated at different temperatures: (a) 700 °C, (b) 750 °C, (c) 800 °C and (d) 850 °C.

where $h = \omega_{i+1} - \omega_i$ and if data interval g is an odd number then $i = 2, 4, 6, \ldots, g - 1, g + 1, \ldots$, while if g is an even number then $i = 1, 3, 5, \ldots, g - 1, g + 1, \ldots$

3.4. Optical constants spectrum

3.4.1. Reflectance and phase change

The reflectance, R, and the phase change, φ, spectrum from $400 \, \text{cm}^{-1}$ to $1000 \, \text{cm}^{-1}$ for PMN–PT powder calcinated at different temperatures is shown in Fig. 6. The values of R and φ change as the temperature increase and the peak value of R is shifted to higher wavenumber.

3.4.2. Refractive index and extinction coefficient

Fig. 7 shows the refractive index, n, and extinction coefficient, k, from $400 \, \text{cm}^{-1}$ to $1000 \, \text{cm}^{-1}$ for PMN–PT powder calcinated at different temperatures. The values of refractive index are not constant and vary as temperature changes. The strong decrease in the refractive index is associated with the fundamental band gap absorption. However,

increasing calcinated temperature does not shift strongly the peak values of n against wavenumber. As a result the shift of refractive index of samples occurred irregularly as shown in Fig. 7.

3.4.3. Dielectric function

As it can be seen from Fig. 7 increasing the temperature causes to change the value of extinction coefficient. The real (ε') and imaginary (ε'') parts of the complex dielectric function ($\tilde{\varepsilon}(\omega) = \varepsilon'(\omega) + i\varepsilon''(\omega)$) can be evaluated from following relations:

$$\varepsilon'(\omega) = n^2(\omega) - k^2(\omega) \tag{8}$$

$$\varepsilon''(\omega) = 2n(\omega)k(\omega) \tag{9}$$

The real and the imaginary parts of the dielectric function for the PMN–PT powder calcinated at different temperatures is shown in Fig. 8. The curves are fairly flat in the long-wavenumber region and rise rapidly at $606 \, \text{cm}^{-1}$. Similar
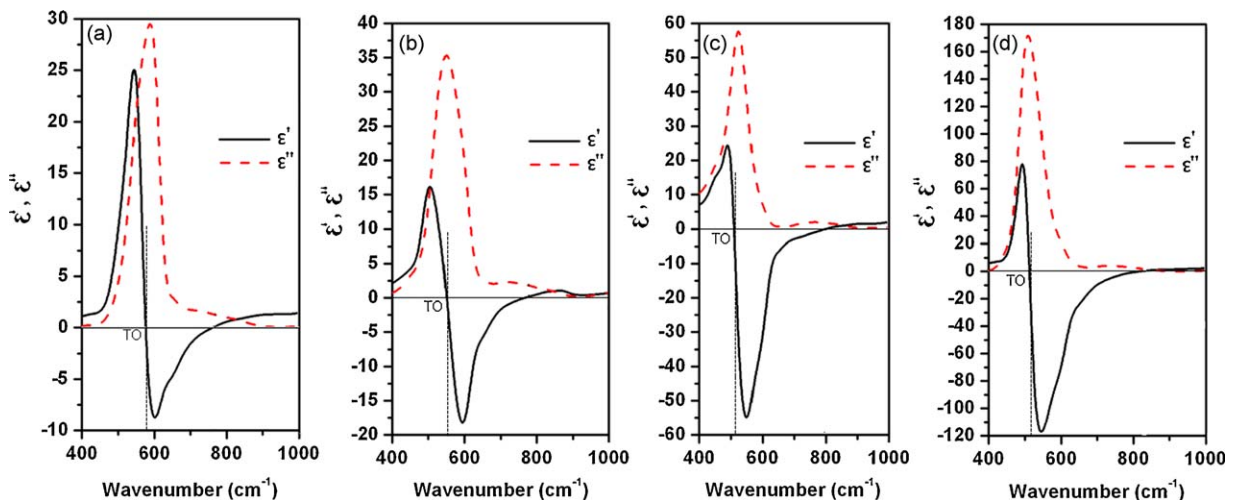
Fig. 8. The real and the imaginary parts for PMN–PT powder calcinated at different temperatures: (a) 700 °C, (b) 750 °C, (c) 800 °C and (d) 850 °C.
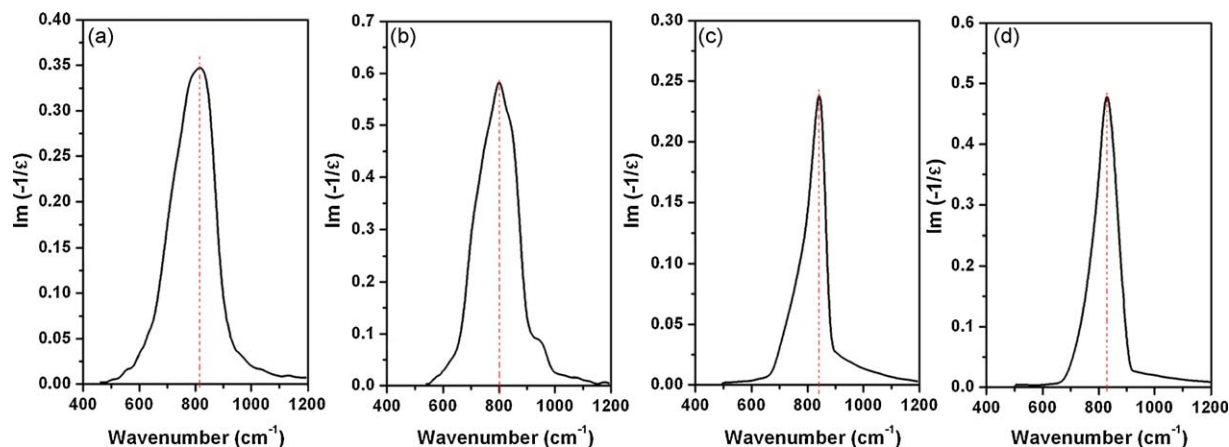
Fig. 9. The spectrum of $\mathrm{Im}(-1/\varepsilon)$ for PMN–PT powder calcinated at different temperatures: (a) 700 °C, (b) 750 °C, (c) 800 °C and (d) 850 °C.

Table 2
IR spectra of optical phonon for PMN–PT powders treated at different temperatures.

	Temperature (°C)			
	700	750	800	850
Transverse optical phonon (TO) (cm^{-1})	569	551	528	512
Longitudinal optical phonon (LO) (cm^{-1})	793	799	852	832

results have also been obtained by Greenler [28], Francis and Ellison [29].

In IR spectrum study, the optical phonons (LO and TO) are the frequencies of interest for describing the optical interactions with the lattice. In general, these interactions will lead to a characteristic optical, i.e. the sharp increase of reflectance caused by the resonance of transverse optical phonon (TO) and decrease at the resonance of the longitudinal optical phonon (LO).

From the above discussion, once the phase $\varphi(\omega)$ value is obtained, the optical and dielectric constants can be determined from numerical calculation of Eqs. (5)–(10). Consequently, the TO and LO mode can be easily determined from the maximum position of ε'' and from the peak position of $\mathrm{Im}(-1/\varepsilon)$ curves, respectively as shown in Fig. 9.

The transverse and longitudinal optical phonons of PMN–PT powder calcinated at different temperatures are presented in Table 2.

4. Conclusions

The PMN–PT nanopowder has been synthesized by the gel-combustion method using citric acid as complexing reagent. The XRD patterns do not indicate the presentation of any impurity phase in 850 °C and free from pyrochlore phase. At temperature of 850 °C the monoclinic and rhombohedra phases coexist. According to the TEM image the average particles size was estimated to be about 20 nm. The optical properties of the PMN–PT have been investigated by transmittance measurements in the range of 400–5000 cm^{-1}. The higher frequency

asymmetric band with a center in the vicinities of 596 cm^{-1} is a composition of $\nu_1\text{-NbO}_3$, $\nu_1\text{-TiO}_3$ and $\nu_1\text{-MgO}_3$ stretching normal vibration modes along the spontaneous polarization in PMN–PT structure. We have presented a detailed description of the use of Kramers–Kronig method to evaluate the optical constants of nanopowders.

References

[1] L.E. Cross, Relaxor ferroelectrics: an overview, Ferroelectrics 151 (1994) 305–320.
[2] A.K. Singh, D. Pandey, Evidence for M_B and M_C phases in the morphotropic phase boundary region of $(1 - x)[\text{Pb}(\text{Mg}_{1/3}\text{Nb}_{2/3})]–x\text{PbTiO}_3$: a Rietveld study, Phys. Rev. B 67 (2003), 064102(1)–064102(12).
[3] B. Noheda, J.A. Gonzalo, L.E. Cross, R. Guo, S.E. Park, D.E. Cox, G. Shirane, Tetragonal-to-monoclinic phase transition in a ferroelectric perovskite: the structure of $\text{PbZr}_{0.52}\text{Ti}_{0.48}\text{O}_3$, Phys. Rev. B 61 (2000) 8687–8695.
[4] S.E. Park, T.R. Shrout, Ultrahigh strain and piezoelectric behavior in relaxor based ferroelectric single crystals, J. Appl. Phys. 82 (1997) 1804–1811.
[5] T.R. Shrout, Z.P. Chang, N. Kim, S. Markgraf, Dielectric behavior of single crystals near the lead magnesium niobate–lead titanate $(1 - x)\text{Pb}(\text{Mg}_{1/3}\text{Nb}_{2/3})\text{O}_3–(x)\text{PbTiO}_3)$ morphotropic phase boundary, Ferroelectrics Lett. Sect. 12 (1990) 63–69.
[6] M. Algueró, C. Alemanya, B. Jiméneza, J. Holcb, M. Kosecb, L. Pardoa, Piezoelectric PMN–PT ceramics from mechanochemically activated precursors, J. Eur. Ceram. Soc. 24 (2004) 937–940.
[7] L.B. Kong, J. Ma, W. Zhu, O.K. Tan, Transluant PMN and PMN–PT ceramics from high-energy ball milling derived powders, Mater. Res. Bull. 37 (2002) 23–32.
[8] C.-H. Lee, S.-I. Kim, Preparation of $\text{Pb}(\text{Mg}_{1/3}\text{Nb}_{2/3})\text{O}_3\text{-PbTiO}_3$ thin films by MOCVD using ultrasonic nebulization, J. Electroceram. 17 (2006) 57–160.
[9] K.R. Udayakumar, J. Chen, V. Kumar, S.B. Krupanidhi, L.E. Cross, Fabrication and characterization of PMN–PT thin films, in: Applications of Ferroelectrics, 1990, IEEE 7th International Symposium on volume, issue, 6–8, June, 1990, 744–746.
[10] S. Kwon, E.M. Sabolsky, G.L. Messing, Low-temperature reactive sintering of 0.65PMN–0.35PT, J. Am. Ceram. Soc. 84 (2001) 648–650.
[11] H. Luo, W.Y. Shih, W.H. Shih, Double precursor solution coating approach for low-temperature sintering of $[\text{Pb}(\text{Mg}_{1/3}\text{Nb}_{2/3})\text{O}_3]_{0.63}[\text{PbTiO}_3]_{0.37}$ solids, J. Am. Ceram. Soc. 90 (2007) 3825–3829.
[12] A.K. Singh, D. Pandey, Evidence for Mb and Mc phases in the morphotropic phase boundary region of $(1 - x)\text{Pb}(\text{Mg}_{1/3}\text{Nb}_{2/3})\text{O}_3–x\text{PbTiO}_3$, Phys. Rev. B 67 (2003), 064102(1)–064102(12).

[13] J.M. Kiat, Y. Uesu, B. Dkhil, M. Matsuda, Ch. Malibert, G. Calvarin, Monoclinic structure of unpoled morphotropic high piezoelectric PMN–PT and PZN-PT compounds, Phys. Rev. B 65 (2002), 064106(1)–064106(4).

[14] C.H. Perry, B.N. Khanna, G. Rupprecht, Infrared studies of perovskite titanate, Phys. Rev. 135 (1964) A408–A412.

[15] J.T. Last, Infrared-absorption studies on barium titanate and related materials, Phys. Rev. 105 (1957) 1740–1750.

[16] W.G. Spitzer, R.C. Miller, D.A. Kleinman, L.E. Howarth, Far infrared dielectric dispersion in BaTiO$_3$, SrTiO$_3$ and TiO$_2$, Phys. Rev. 126 (1962) 1710–1712.

[17] C.A. Sergides, A.R. Chughtai, D.M. Smith, Determination of optical constants of polymer films using a Fourier transform infrared reflection method, polyethylene terephthalate (PET), Appl. Spectrosc. 41 (1987) 154–157.

[18] R.T. Graf, J.L. Koenig, H. Ishida, Optical constant determination of thin polymer films in the infrared, Appl. Spectrosc. 39 (1985) 405–408.

[19] M. Ghasemifard, S.M. Hosseini, A. Khorsand Zak, Gh.H. Khorrami, Microstructural and optical characterization of PZT nanopowder prepared at low temperature, Physica E 41 (2009) 418–422.

[20] R. Swanepoel, Determination of the thickness and optical constants of amorphous silicon, J. Phys. E: Sci. Instrum. 16 (1983) 1214–1222.

[21] P. Prathap, Y.P.V. Subbaiah, M. Devika, K.T. Ramakrishna Reddy, Optical properties of In$_2$O$_3$ films prepared by spray pyrolysis, Mater. Chem. Phys. 100 (2006) 375–379.

[22] R.H. Bube, Electronic Properties of Crystalline Solids, Academic Press, New York, 1974, Chapter 11.

[23] F. Stern, Elementary optical properties of solids, Solid State Phys. 15 (1963) 327–340.

[24] H.R. Philipp, E.A. Taft, Optical constants of Germanium in the region 1 to 10 eV, Phys. Rev. 113 (1959) 1002–1005.

[25] D.M. Roessler, Kramers-Kronig analysis of reflection data. III. Approximations, with reference to sodium iodide, Br. J. Appl. Phys. 17 (1966) 1313–1317.

[26] D.M. Roessler, Kramers–Kronig analysis of reflection data, Br. J. Appl. Phys. 16 (1965) 1119–1123.

[27] M. Abramowitz, I.A. Stegun, Handbook of Mathematical Functions, Dover, New York, 1965.

[28] R.G. Greenler, Reflection absorption infrared spectroscopy and the structure of molecular adsorbents on metal surfaces, J. Chem. Phys. 51 (2000) 381–403.

[29] S.A. Francis, A.H. Ellison, Infrared spectra of monolayers on metal mirrors, J. Opt. Soc. Am. 49 (1959) 131–137.